2015-02-13

Experimental measurements of the spectral absorption coefficient of pure fused silica optical fibers

Travis J. Moore
Brigham Young University - Provo, travisjmoore@gmail.com

Matthew R. Jones
Brigham Young University - Provo, mrjones@byu.edu

Experimental measurements of the spectral absorption coefficient of pure fused silica optical fibers

Travis J. Moore* and Matthew R. Jones

Department of Mechanical Engineering, Brigham Young University, 435 Crabtree Building, Provo, Utah 84602, USA

*Corresponding author: travisjmoore@gmail.com

Received 1 October 2014; revised 16 December 2014; accepted 14 January 2015;
posted 14 January 2015 (Doc. ID 223842); published 0 MONTH 0000

Knowledge of the spectral absorption coefficient of fused silica optical fibers is important in modeling heat transfer in the processes and applications in which these fibers are used. An experimental method used to measure the spectral absorption coefficient of optical fibers is presented. Radiative energy from a blackbody radiator set at different temperatures is directed through the optical fibers and into an FTIR spectrometer. Spectral instrument response functions are calculated for different fiber lengths. The ratios of the slopes of the instrument response functions for the different lengths of fibers are used to solve for the spectral absorption coefficient of the fibers. The spectral absorption coefficient of low OH pure fused silica optical fibers is measured between the wavelengths 1.5 and 2.5 μm. © 2015 Optical Society of America

OCIS codes: (060.2400) Fiber properties; (060.2310) Fiber optics; (300.6300) Spectroscopy, Fourier transforms.

http://dx.doi.org/10.1364/AO.99.099999

1. Introduction

Knowledge of the spectral absorption coefficient of fused silica optical fibers is important in modeling heat transfer in the processes and applications in which these fibers are used. These include optical fiber thermometers [1–6], the splicing of optical fibers using lasers [7], the fabrication of fiber couplers and tapers [8], and the manufacture of optical fibers by drawing [9–13]. Myers [14] introduced a two-band model of the spectral absorption coefficient of fused silica that has been widely used to model heat transfer in optical fiber drawing processes [9–12]. This model neglects absorption at wavelengths less than 3 μm. However, Wei *et al.* [13] showed that the absorption in the short wavelength region is not negligible.

Various methods have been used to measure the absorption coefficient of fused silica. Izawa *et al.* measured the spectral absorption coefficient of fused silica between wavelengths of 2.5 and 25 μm using a scanning grating spectrometer [15,16]. Yoshida *et al.* estimated the absorption coefficient of fused silica at a wavelength of 1.06 μm by fitting thermal lensing measurements using a Shack–Hartmann wave-front detector to a model based on the temperature dependencies of the refractive index and the thermal expansion coefficient [17]. However, no measurements have been reported over the spectral band between 1.5 and 2.3 μm.

Here, the spectral absorption coefficient of low OH pure fused silica optical fibers is measured between the wavelengths of 1.5 and 2.5 μm by directing radiative energy from a blackbody radiator at different temperatures through the optical fibers and into an FTIR spectrometer. Spectral instrument response functions are created for different fiber lengths. The ratios of the slopes of the spectral instrument response function for the different lengths of fibers are used to solve for the spectral absorption coefficient of the fibers.

1559-128X/15/070001-01$15.00/0

2. Experimental Setup

The experimental setup used to measure the spectral absorption coefficient of optical fibers is shown in Fig. 1.

Radiative energy from a blackbody calibration source [18] was directed into an optical fiber through a reflective collimator [19]. The collimator consists of a 90° off-axis parabolic mirror with a protected silver coating that collects collimated radiant energy and directs it into the end of the optical fiber. The average reflectance of the mirror is greater than 96% between the wavelengths of 0.45 and 20 μm. The fiber connects to the collimator with an SMA connector. The other end of the optical fiber was connected by an SMA connector to another reflective collimator, which collimates the radiation from the fiber and directs it into the external access port of an FTIR spectrometer [20]. The FTIR spectrometer collects the radiant energy and outputs a spectral signal. The optical fibers used in this research are multimode step-index low OH fibers with a 400 μm diameter pure fused silica core, a 440 μm diameter fluorine doped fused silica cladding, a 470 μm diameter polyimide coating, and a 700 μm diameter tefzel jacket [21]. The fibers have a numerical aperture of 0.22.

3. Instrument Response Function

The FTIR spectrometer was equipped with a deuterated triglycine sulfate (DTGS) pyroelectric detector. Infrared radiation incident on the detector increases the detector temperature, which changes the dielectric constant of the deuterated triglycine sulfate. The change in capacitance with temperature is measured as a voltage across the detector element [22]. The spectral response of a DTGS detector has been shown to be linear [22–25]. The spectral irradiation incident on the detector, $G_{\lambda,D}$, is related to the detector signal, M_λ, as follows:

$$G_{\lambda,D} = A_\lambda M_\lambda + B_\lambda. \tag{1}$$

The offset term, B_λ, includes radiation emitted by the collecting optical system and by the detector itself [22–25]. The spectral irradiation incident on the detector is [26]

$$G_{\lambda,D} = \int_{2\pi} I_{\lambda,D} \cos\theta_D \, d\Omega, \tag{2}$$

where $I_{\lambda,D}$ is the spectral radiative intensity incident on the detector, and θ_D is the angle between the incident ray and the normal to the detector surface. Assuming that the collimated radiation from the reflective collimator into the FTIR spectrometer is the only source of radiative energy and that the solid angle subtended by the collimator when viewed from the detector, $\Delta\Omega_{D\to C}$, is small, Eq. (2) reduces to

$$G_{\lambda,D} \approx I_{\lambda,D} \Delta\Omega_{D\to C}. \tag{3}$$

The spectral intensity incident on the detector is directly proportional to the spectral intensity exiting the fiber,

$$I_{\lambda,D} = P_\lambda I_{\lambda,f}, \tag{4}$$

where P_λ represents attenuation along the optical path due to reflections and transmission through components in the collimator and the FTIR. An equation representing the spectral intensity exiting the fiber, $I_{\lambda,f}$, can be obtained by solving the radiative transfer equation (RTE) in the fiber. Figure 2 shows a schematic of the coordinate system used to determine $I_{\lambda,f}$.

The fiber is assumed to be an emitting, absorbing, nonscattering medium. In order to account for the multiple reflections of a beam which occur within an optical fiber, it is easier to consider the intensity at a given point z in the $\hat{s}$ direction from a point source in the fiber as that coming from an image of this point projected onto the boundary a distance z_s from the reception point, as illustrated in Fig. 2 [27]. Therefore, the optical fiber can be treated as a one-dimensional medium of length L.

An integrating factor is used to solve the RTE for the spectral intensity in the positive direction, I_λ^+, for which $0 < \theta < \pi/2$, and for that in the negative direction, I_λ^-, for which $\pi/2 < \theta < \pi$. The intensity at $z = 0$ is the blackbody intensity coming from the blackbody radiator. The intensity at $z = L$ is that which is reflected from the interface between the fiber and the air. The details of this solution can be found in [28]. The spectral radiative intensity exiting the fiber is equal to the portion of the intensity at $z = L$ which is transmitted through the end of the fiber. It is shown in the following equation:

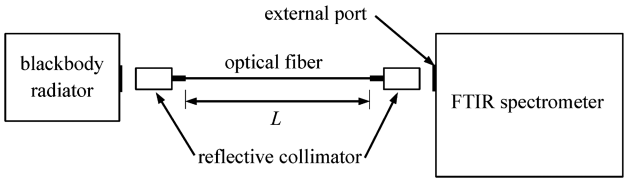

F1:1 F1:2 Fig. 1. Schematic of the experimental setup used to measure the spectral absorption coefficient of optical fibers.

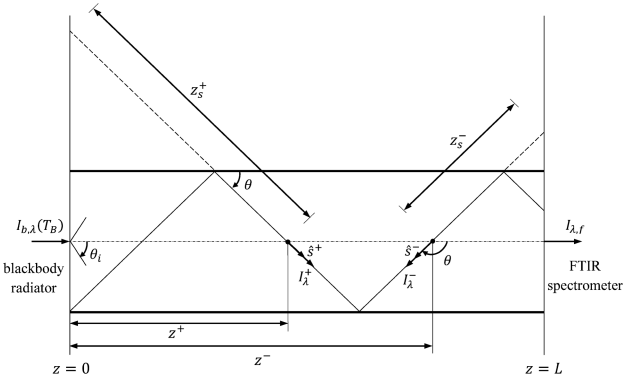

F2:1 F2:2 Fig. 2. Coordinate system used to determine the spectral intensity exiting the fiber.

$$I_{\lambda,f} = \tau_{\lambda,L}\int_{\mu_i}^{1}\left(I_{b,\lambda}(T_B)e^{-\kappa_\lambda L/\mu} + \frac{\kappa_\lambda}{\mu}\int_0^L I_{b,\lambda}(T(z'))e^{-\kappa_\lambda(L-z')/\mu}\mathrm{d}z'\right)\mathrm{d}\mu. \quad (5)$$

In Eq. (5), $\tau_{\lambda,L}$ is the spectral transmittance at the right boundary of the optical fiber. The first term in the parentheses of Eq. (5) represents the spectral blackbody intensity coming from the blackbody radiator at the blackbody radiator temperature, T_B. This radiative energy decreases along the length of the optical fiber due to absorption, where κ_λ is the spectral absorption coefficient of the fiber, and L is the length of the fiber. The second term in parentheses represents the contribution to the total incident intensity on the detector due to emission from the fiber. This is dependent upon the temperature profile along the fiber, $T(z)$. Both of these terms are integrated over the direction cosine, $\mu = \cos\theta$, between $\cos\theta_i$ and $\cos 0 = 1$ where θ_i is the critical angle that forms the acceptance cone inside of which total internal reflection occurs in the fiber. The angle θ is measured from the fiber axis. In the experimental setup used here, the entire fiber was at room temperature, so the integral on the right hand side of Eq. (5) is easily calculated.

$$I_{\lambda,D} = P_\lambda\tau_{\lambda,L}\int_{\mu_i}^{1}(I_{b,\lambda}(T_B)e^{-\kappa_\lambda L/\mu} + I_{b,\lambda}(T_\infty)(1-e^{-\kappa_\lambda L/\mu}))\mathrm{d}\mu. \quad (6)$$

Substituting Eq. (6) into Eq. (3), substituting the result into Eq. (1) and rearranging gives

$$I_{b,\lambda}(T_B) = C_\lambda M_\lambda + D_\lambda, \quad (7)$$

where

$$C_\lambda = \frac{A_\lambda}{P_\lambda\tau_{\lambda,L}\Delta\Omega_{D\to C}\int_{\mu_i}^{1}e^{-\kappa_\lambda L/\mu}\mathrm{d}\mu}, \quad (8)$$

and

$$D_\lambda = \frac{B_\lambda}{P_\lambda\tau_{\lambda,L}\Delta\Omega_{D\to C}\int_{\mu_i}^{1}e^{-\kappa_\lambda L/\mu}\mathrm{d}\mu} - \frac{I_{b,\lambda}(T_\infty)}{P_\lambda\tau_{\lambda,L}\Delta\Omega_{D\to C}\int_{\mu_i}^{1}e^{-\kappa_\lambda L/\mu}\mathrm{d}\mu}\int_{\mu_i}^{1}(1-e^{-\kappa_\lambda L/\mu})\mathrm{d}\mu. \quad (9)$$

In Eq. (7), C_λ and D_λ are the terms of the instrument response function for the experimental setup shown in Fig. 1. These are dependent on the length of the fiber. For a given fiber length, the instrument response function can be determined by collecting spectral measurements, M_λ, with the FTIR spectrometer at various blackbody radiator temperatures. The spectral blackbody intensity can be calculated using the Planck function [26] and linear curves fit to these intensities as a function of M_λ [28]. For each wavelength, the slope of the linear fit is given by C_λ, and the offset is given by D_λ.

4. Experiments

The spectral instrument response function was determined using the process described above for four different lengths of optical fibers: 0.5, 1, 1.5, and 2 m. For each fiber length, spectral measurements were collected using the FTIR spectrometer at six blackbody radiator temperatures between 500°C and 1200°C. Each spectrum collected by the FTIR spectrometer represents an average of 32 scans at a resolution of 32 cm^{-1}. In order to account for variability in the experiments, at each blackbody temperature each of the fibers was secured between the two reflective collimators, and the measurements were repeated five times. The average of these five signals at each temperature was used to create the instrument response function for each fiber length.

The ratio of the slope terms, C_λ, of the instrument response function given in Eq. (8) for two different fiber lengths L_1 and L_2 is

$$\frac{C_{\lambda,1}}{C_{\lambda,2}} = \frac{\frac{A_\lambda}{P_\lambda\tau_{\lambda,L}\Delta\Omega_{D\to C}\int_{\mu_i}^{1}e^{-\kappa_\lambda L_1/\mu}\mathrm{d}\mu}}{\frac{A_\lambda}{P_\lambda\tau_{\lambda,L}\Delta\Omega_{D\to C}\int_{\mu_i}^{1}e^{-\kappa_\lambda L_2/\mu}\mathrm{d}\mu}}. \quad (10)$$

The P_λ and $\Delta\Omega_{D\to C}$ terms are functions of the optical setup of the experiment, and the A_λ term is a function of the detector. Each of these terms remains constant throughout the experiment. Therefore, if each of the fibers is assumed to have the same spectral absorption coefficient and acceptance cone, Eq. (10) can be simplified to

$$\frac{C_{\lambda,1}}{C_{\lambda,2}} = \frac{\int_{\mu_i}^{1}e^{-\kappa_\lambda L_2/\mu}\mathrm{d}\mu}{\int_{\mu_i}^{1}e^{-\kappa_\lambda L_1/\mu}\mathrm{d}\mu}. \quad (11)$$

The only unknown in Eq. (11) is the spectral absorption coefficient of the fiber, κ_λ. The spectral absorption coefficient can be determined from Eq. (11) using optimization methods. The least squares norm of the difference between the left side and the right side of Eq. (11) is minimized by adjusting the values of κ_λ at the wavelengths at which measurements are made. The integrals on the right side of Eq. (11) are evaluated numerically.

The solver application in Microsoft Excel was used to find the maximum likelihood estimate of the spectral absorption coefficient in Eq. (11) using the ratios of the slopes of the instrument response function of every combination of the four fibers.

5. Results and Discussion

The average spectral absorption coefficient of the optical fibers calculated from all of the experiments is shown in Fig. 3. The error bars represent one standard deviation from the average. The spectral

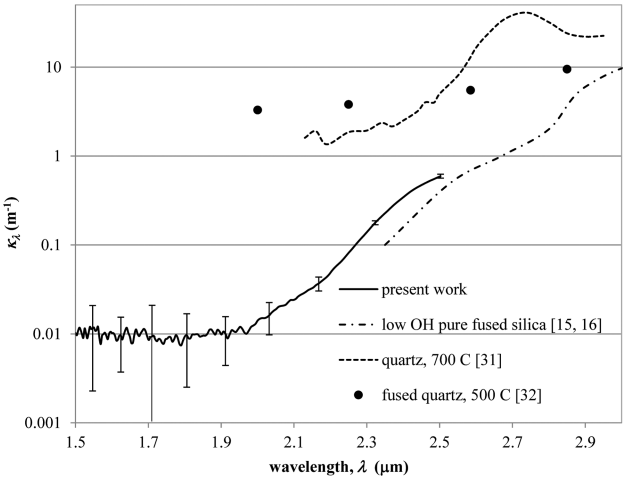

F3:1 F3:2 F3:3 Fig. 3. Measurements of the spectral absorption coefficient of low OH fused silica optical fibers, low OH fused silica [15,16], quartz [31], and fused quartz [32].

measurements were made between 1.5 μm (the lower limit of the detector) and 2.5 μm (the upper limit of the transmission range of the fibers). The refractive index of silica is relatively constant over this spectral band [29]. Therefore, in Eq. (11), it was assumed that the critical angle does not vary with wavelength. Figure 3 also shows spectral absorption coefficient measurements of low OH fused silica made by Izawa and co-workers [15,16], which compare favorably with those made in this work. The measurements made in this work are also consistent with the measured value of 0.0018 m^{-1} at 1.06 μm made by Yoshida *et al.* [17] and the reported value of 0.001 m^{-1} at 1 μm [30].

For reference, measurements of the spectral absorption coefficients of quartz at 700°C [31], and fused quartz at 500°C [32] are also shown in Fig. 3. All data shown in Fig. 3 were found from published data using data extraction software. The absorption coefficient of the low OH fused silica fibers measured here follows the same trends as that of the quartz and fused quartz but is significantly lower. This may be a result of the water content in the glass or the fact that the measurements in [31] and [32] were made at elevated temperatures. Moisture present in the manufacturing process results in hydroxyl groups chemically bonded to the silica network (SiOH), which increase the transmission loss in the fibers [33]. Additionally, as shown by research performed on fused quartz, the spectral absorption coefficient of glasses increases with increasing temperature [32,34].

6. Conclusion

An experimental method used to measure the spectral absorption coefficient of optical fibers was presented in which radiative energy from a blackbody radiator is directed through the optical fibers and into an FTIR spectrometer. Spectral instrument response functions are calculated for different fiber lengths, and the ratios of the slopes of these functions for the different lengths of fibers are used to estimate the spectral absorption coefficient of the fibers. The spectral absorption coefficient of low OH pure fused silica optical fibers was measured between 1.5 and 2.5 μm. The spectral absorption coefficient of low OH pure fused silica has not previously been reported between 1.5 and 2.3 μm. The measurement technique is relatively simple and may be readily used to measure spectral absorption coefficients in other fibers of interest. The measurements were consistent with previous results reported between 2.3 and 2.5 μm.

References

1. R. R. Dils, "High-temperature optical fiber thermometer," J. Appl. Phys. **54**, 1198–1201 (1983).
2. W. S. Cheung, "The development of an optical fibre thermometer for gas turbine engines," Sens. Actuators **19**, 105–117 (1989).
3. M. R. Jones and D. G. Barker, "Use of blackbody optical fiber thermometers in high temperature environments," J. Thermophys. Heat Transfer **16**, 306–312 (2002).
4. D. G. Barker and M. R. Jones, "Temperature measurements using a high-temperature blackbody optical fiber thermometer," ASMEJ Heat Transfer **125**, 471–477 (2003).
5. D. G. Barker and M. R. Jones, "Inversion of spectral emission measurements to reconstruct the temperature profile along a blackbody optical fiber thermometer," Inverse Probl. Eng. **11**, 495–513 (2003).
6. D. J. Frankman, B. W. Webb, and M. R. Jones, "Investigation of lightpipe volumetric radiation effects in RTP thermometry," ASMEJ Heat Transfer **128**, 132–141 (2006).
7. H. Fujita, Y. Suzaki, and A. Tachibaan, Method of splicing optical fibers by CO_2 Laser, U.S. Patent 4263495 (April 1981).
8. T. E. Dimmick, G. Kakarantzas, T. A. Birks, and P. St. J. Russell, "Carbon dioxide laser fabrication of fused-fiber couplers and tapers," Appl. Opt. **38**, 6845–6848 (1999).
9. J. Liu, S. J. Zhang, and Y. S. Chen, "Advanced simulation of optical fiber drawing process," Num. Heat Transfer Part A Applications **40**, 473–795 (2001).
10. M. Taroni, C. J. W. Breward, L. J. Cummings, and I. M. Griffiths, "Asymptotic solutions of glass temperature profiles during steady optical fibre drawing," J. Eng. Math. **80**, 1–20 (2013).
11. C. Chunming and Y. Jaluria, "Numerical simulation of transport in optical fiber drawing with core-cladding structure," ASMEJ Heat Transfer **129**, 559–567 (2007).
12. Z. Wei, K. Lee, Z. Zhou, and S. Hong, "Modeling of advanced melting zone for manufacturing of optical fibers," J. Manuf. Sci. Eng. Trans. ASME **126**, 377–387 (2004).
13. Z. Wei, K. Lee, S. W. Tchikanda, Z. Zhou, and S. Hong, "Effects of radiative transfer modeling on transient temperature distribution in semitransparent glass rod," ASMEJ Heat Transfer **125**, 635–643 (2003).
14. M. R. Myers, "A model for unsteady analysis of preform drawing," AIChE J. **35**, 592–602 (1989).
15. T. Izawa, N. Shibata, and A. Takeda, "Optical attenuation in pure and doped fused silica in the IR wavelength region," Appl. Phys. Lett. **31**, 33–34 (1977).
16. T. Izawa and S. Sudo, *Optical Fibers: Materials and Fabrication* (KTK Scientific, 1987).
17. S. Yoshida, D. H. Reitze, D. B. Tanner, and J. D. Mansell, "Method for measuring small optical absorption coefficients with use of a Shack–Hartmann wave-front detector," Appl. Opt. **42**, 4835–4840 (2003).
18. Landcal R1200P, www.landinst.com.
19. RC12SMA-P01, www.thorlab.us.
20. Nicolet 8700 FT-IR Spectrometer, www.thermo.com.
21. SIR400/440PIT, www.fibertech-optica.com.
22. E. Lindermeir, P. Haschberger, C. Tank, and H. Dietl, "Calibration of a Fourier transform spectrometer using three blackbody sources," Appl. Opt. **31**, 4527–4533 (1992).

23. P. C. Dufour, N. L. Rowell, and A. G. Steele, "Fourier-transform radiation thermometry: measurements and uncertainties," Appl. Opt. **37**, 5923–59314 (1998).
24. L. González-Fernández, R. B. Pérez-Sáez, L. del Campo, and M. J. Tello, "Analysis of calibration methods for direct emissivity measurements," Appl. Opt. **49**, 2728–2735 (2010).
25. T. J. Moore and M. R. Jones, "An experimental method for making spectral emittance and surface temperature measurements of opaque surfaces," J. Quant. Spectry. Radiative Transfer **112**, 1191–1196 (2011).
26. M. F. Modest, *Radiative Heat Transfer*, 2nd ed., (Academic, 2003).
27. V. S. Yuferev, "Radiation-conduction heat transfer in a thin semitransparent cylinder in the light-guide approximation," J. Appl. Mech. Tech. Phys. **20**, 415–418 (1980).
28. T. J. Moore, "Application of variation of parameters to solve nonlinear multimode heat transfer problems," PhD dissertation, Brigham Young University, Provo, UT (2014).
29. R. Kitamura, L. Pilon, and M. Jonasz, "Optical constants of silica glass from extreme ultraviolet to far infrared at near room temperature," Appl. Opt. **46**, 8118–8133 (2007).
30. http://www.crystran.co.uk/optical-materials/silica-glass-sio2.
31. E. Loenen and L. van der Tempel, *Determination of Absorption Coefficients of Glasses at High Temperatures, by Measuring the Thermal Emission* (Philips Electronics N. V., 1996).
32. E. C. Beder, C. D. Bass, and W. F. Shackleford, "Transmissivity and absorption of fused quartz between 0.22 m 3.5 m from room temperature to 1500 degrees C," Appl. Opt. **10**, 2263–2268 (1971).
33. O. Humbach, H. Fabian, U. Grzesik, U. Haken, and W. Heitmann, "Analysis of OH absorption bands in synthetic silica," J. Non-Cryst. Solids **203**, 19–26 (1996).
34. L. V. Prikhodk and Kh. S. Bagdasarov, "Temperature dependence of IR absorption in fused quartz at high temperatures," Optika i spektroskopiâ **34**, 1210–1211 (1973).

Queries

1. AU: Should this aperture value have a unit of measurement?

2. A check of online databases revealed a possible error in this reference. The year has been changed from '1979' to '1980'. Please confirm this is correct.